An epitaxial perovskite as a compact neuristor

Salverda, M.; Hamming-Green, R. P.; Noheda, B.

Published in:
Journal of Physics D: Applied Physics

DOI:
10.1088/1361-6463/ac71e2

Publication date:
2022

PAPER • **OPEN ACCESS**

An epitaxial perovskite as a compact neuristor: electrical self-oscillations in $TbMnO_3$ thin films

To cite this article: M Salverda *et al* 2022 *J. Phys. D: Appl. Phys.* **55** 335305

OPEN ACCESS
IOP Publishing
Journal of Physics D: Applied Physics
J. Phys. D: Appl. Phys. **55** (2022) 335305 (8pp)
https://doi.org/10.1088/1361-6463/ac71e2

An epitaxial perovskite as a compact neuristor: electrical self-oscillations in $TbMnO_3$ thin films

M Salverda[1,*], R P Hamming-Green[1,2] and B Noheda[1,2,*]

[1] Zernike Institute for Advanced Materials, University of Groningen, 9747 AG Groningen, The Netherlands
[2] CogniGron Center, University of Groningen, 9747 AG Groningen, The Netherlands

E-mail: m.salverda@rug.nl and b.noheda@rug.nl

Received 16 March 2022, revised 8 May 2022
Accepted for publication 20 May 2022
Published 7 June 2022

Abstract

Developing materials that can lead to compact versions of artificial neurons (neuristors) and synapses (memristors) is the main aspiration of the nascent neuromorphic materials research field. Oscillating circuits are interesting as neuristors, as they emulate the firing of action potentials. Here we present room-temperature self-oscillating devices fabricated from epitaxial thin films of semiconducting $TbMnO_3$. We show that the negative differential resistance regime observed in these devices, orginates from transitions across the electronic band gap of the semiconductor. The intrinsic nature of the mechanism governing the oscillations gives rise to a high degree of control and repeatability. Obtaining such properties in an epitaxial perovskite oxide opens the way towards combining self-oscillating properties with those of other piezoelectric, ferroelectric, or magnetic perovskite oxides in order to achieve hybrid neuristor-memristor functionality in compact heterostructures.

Supplementary material for this article is available online

Keywords: negative differential resistance, terbium manganite, self-oscillators, artificial neurons

(Some figures may appear in colour only in the online journal)

1. Introduction

Current-controlled negative differential resistance (CC-NDR) occurs when the voltage (V) across a material decreases while the current (I) increases. I–V characteristics featuring CC-NDR display a region of voltages, between the threshold voltage, V_{th}, and the holding voltage, V_h, where multiple current values are possible for a single voltage. CC-NDR can be caused by different mechanisms, such as impact ionization [1–3] and metal–insulator transitions [4–7], but also by thermally-activated or thermally-assisted mechanisms, such as Schottky emission and Poole-Frenkel conduction [8–10]. Although materials systems with CC-NDR have been found since the 60s [11–18], the promise of energy-efficient, neuromorphic hardware to perform in-memory and on-edge processing [19–24], has renewed interest and brought about a new wave of research on this phenomenon [4, 25–29]. For instance, selector devices are being implemented in memristor arrays, where the highly non-linear NDR helps to reduce leakage and sneak path currents [30]. CC-NDR is also used to

* Authors to whom any correspondence should be addressed.

construct self-oscillators with regular and chaotic oscillations and to emulate spiking neurons [4, 24, 28, 29, 31–34].

More specifically, current passing through the device causes Joule heating, increasing the temperature of the device as $T = T_{amb} + R_{th}IV$, where R_{th} is the thermal resistance of the device, which includes the heat capacity of the active region and the thermal conductance between the active region and the surrounding material. The increase of the device temperature leads to a decrease in its resistance [3, 35–37]. This will happen for all conduction mechanisms that depend super-linearly on temperature [2, 3, 8], as those mentioned above. There are also conduction mechanisms that are field-dependent, such as avalanche/impact ionization [1–3], often found in semiconductors as well. However, as the current usually increases enormously when these mechanisms are triggered, producing additional Joule heating, they are often difficult to separate from temperature-activated effects [2, 3]. Another well-known mechanism is the Mott metal–insulator transition [4–7], which can be triggered by temperature or electric field.

Although most recent work is focused on binary transition metal-oxide systems, such as TaO_x [25, 38, 39], VO_x [4, 40] and NbO_x [4, 34, 41], the latter two also displaying Mott transitions above room temperature, it is of much interest to demonstrate this behaviour in a wider range of materials. In particular, heterostructures of oxide perovskites are rich in functional properties [42] and memristive and synaptic devices have been fabricated with them [24, 43–47]. Selectors and neuron-like devices made of these materials could allow for heterostructures that combine neuristor and synaptic functionality in a compact manner. However, considering the many mechanisms that can lead to CC-NDR [8], only relatively few perovskite oxides have been shown to exhibit it, and most of these studies were performed at low temperatures [15, 48–50].

Here we present room-temperature CC-NDR in devices fabricated from epitaxial thin films of semiconducting perovskite $TbMnO_3$. No metal–insulator transition or other structural or electronic transitions are known in this material above room temperature. We show that the device can oscillate between HR and LR states and that these electrical and thermal oscillations are maintained with high endurance. The origin of the oscillations is shown to be the thermal promotion of electrons across the band-gap, a mechanism that is currently not sufficiently highlighted in relation with this behaviour. As a consequence of this intrinsic origin, these devices do not require forming steps and allow for a clean and well-controlled device operation.

2. Methods

Following previous work [51–53], epitaxial thin films of $TbMnO_3$ with a thickness of 60 nm were grown on single-terminated Nb-doped $SrTiO_3$ substrates by pulsed laser deposition, using an oxygen pressure of 0.9 mbar, a laser fluence of 2.35 J cm^{-2}, a heater temperature of 750 °C, a target-heater distance of 55 mm and repetition rate of 1 Hz, produced by a 248 nm excimer laser. The films were examined by atomic force microscopy, x-ray diffraction and transmission electron microscopy and showed the same structural characteristics as those in the mentioned papers [51–53].

On top of the film, circular Pt electrodes with a thickness of 80 nm and diameter of 10 μm were fabricated using photolithography and e-beam evaporation. To provide an ohmic contact with the bottom Nb-doped $SrTiO_3$ electrode [54], a layer of Ti (10 nm) was evaporated to the back-side of the substrate, capped with a layer of Pt (50 nm) (see a schematic in the inset of figure 1(a)). Electrical measurements were performed using a Keithley 4200A-SCS parameter analyzer equipped with source measure units (SMUs) and a pulse measure unit, as well as a LeCroy 9410 Oscilloscope.

3. Results

I–V measurements were carried out on $TbMnO_3$ thin films under DC voltages. At low voltages (<1 V), an exponential and rectifying *I–V* dependence is found (see figure 1(a)), originating from the p–n junction at the interface between the p-type $TbMnO_3$ and n-type Nb-doped $SrTiO_3$ [55, 56]. At higher voltages (1 V < V < 1.68 V), the current is limited by series resistances, including that of the $TbMnO_3$ film and the Nb-doped SrTiO3 substrate, and becomes linear in voltage. Above 1.68 V, the transport becomes nonlinear again, ultimately leading to an NDR regime (see figure 1(b)).

Upon increasing the applied voltage above $V_{th} = 1.9$ V in a voltage-controlled experiment, the device switches from its HR state to its LR state. On the return sweep, the OFF-switching (from LR to HR) takes place at $V_h = 1.68$ V. These CC-NDR cycles are displayed in a highly reproducible manner without the need of a forming step. Typical CC-NDR behaviour is observed, with a smooth transition for current-controlled *I–V* measurements (also referred to as S-type NDR), while voltage-controlled measurements show hysteresis. It is worth noticing that the horizontal axes in figure 1 display the device voltage, V_{device}, which is the applied voltage, *V*, corrected for a series resistor, added to prevent current overshoots and the accompanying damage to the device. It should also be noted that a significant voltage (up to 0.9 V) will drop over the p–n junction at the interface, which means that the voltages that are actually applied to the $TbMnO_3$ film are smaller than what is indicated by the horizontal axes of the figures.

Measurements of the resistance of the films show that the electrical transport of $TbMnO_3$ around and above room temperature is thermally activated, following:

$$\rho = \rho_0 \, e^{E_a/k_B T}, \tag{1}$$

with an activation energy E_a of about 0.26 eV (see figure 1(c)), which is consistent with an activation energy across a semiconducting band gap of $E_g = 2E_a \approx 0.5$ eV, in agreement with the reported values in this material [57]. Current passing through the device causes Joule heating, which increases the temperature of the device as $T = T_{amb} + R_{th}IV$, where R_{th} is the thermal resistance of the device, which includes the heat capacity of the active region and the thermal conductance between the active region and the surrounding material. Together with

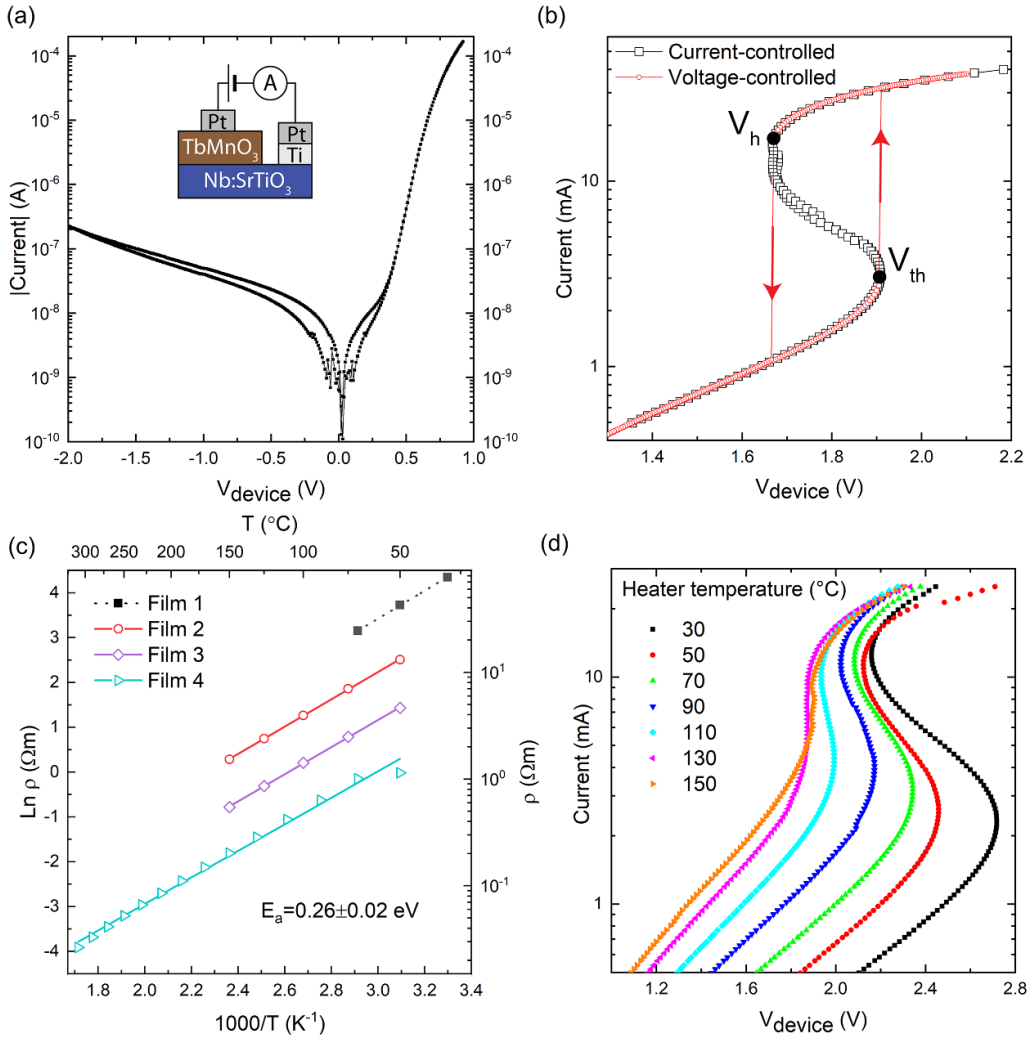

Figure 1. (a) *I*–*V* measurement of an out-of-plane device in the low voltage range; (b) room temperature DC *I*–*V* measurement of a typical $TbMnO_3$ device around the NDR transition. The voltage-controlled measurements (red curve) show the abrupt jump from the high resistance (HR) state to the low resistance (LR) state at V_{th} and vice versa on decreasing V for $V < V_h$. The current-controlled measurements (black curve) show a smooth transition from the HR to the LR state and back; (c) Arrhenius plot of the resistivity of several $TbMnO_3$ films, showing the presence of a single activation energy in films that were grown with various growth parameters. The growth parameters of these films are shown in the supplementary information. Filled symbols are data from out-of-plane impedance measurements, open symbols are from lateral Van der Pauw measurements; (d) current controlled IV measurements at different ambient temperatures, where the temperature was controlled by a heater stage underneath the device.

equation (1), this gives rise to the CC-NDR behaviour. To further show that the heating and subsequent spontaneous cooling of the material causes the reversible hysteretic transition in figure 1(b), the temperature of the device has been increased by external means, as shown in figure 1(d)). It can be observed that at a device temperature of 150 °C, the difference between the HR and LR is already small enough to lead to the disappearance of the NDR, due to the inability of the device to cool-down.

3.1. *Pulsed* I–V *and transient measurements*

A temperature-induced effect requires some settling time, while an electric field effect can happen at a much faster time scale, provided a small electrical RC [58, 59]. Pulsed *I*–*V* measurements can, therefore, be used to attest that thermal processes are at play. Figure 2(a) shows measurements for different pulse lengths, from $\Delta t = 10$ μs to 2 ms. The threshold voltage V_{th} is shown to depend on the pulse width: shorter pulses drive V_{th} to higher values, which is a result of the temperature not reaching its steady-state value. For longer pulse widths, V_{th} approaches a constant value, which indicates that the device temperature is close to the corresponding steady state value.

Interestingly, at higher currents within the NDR region, we observe that the device can further decrease its resistance if the rise time (t_r) of the pulse is short, as shown in the inset of figure 2(b) for $t_r = 1$ μs compared to $t_r = 5$ μs. To investigate the origin of this phenomenon, we perform time-resolved current measurements during the application of voltage pulses with various t_r (see figure 2(b)). These results shows that a smooth transition to a higher current state takes place for

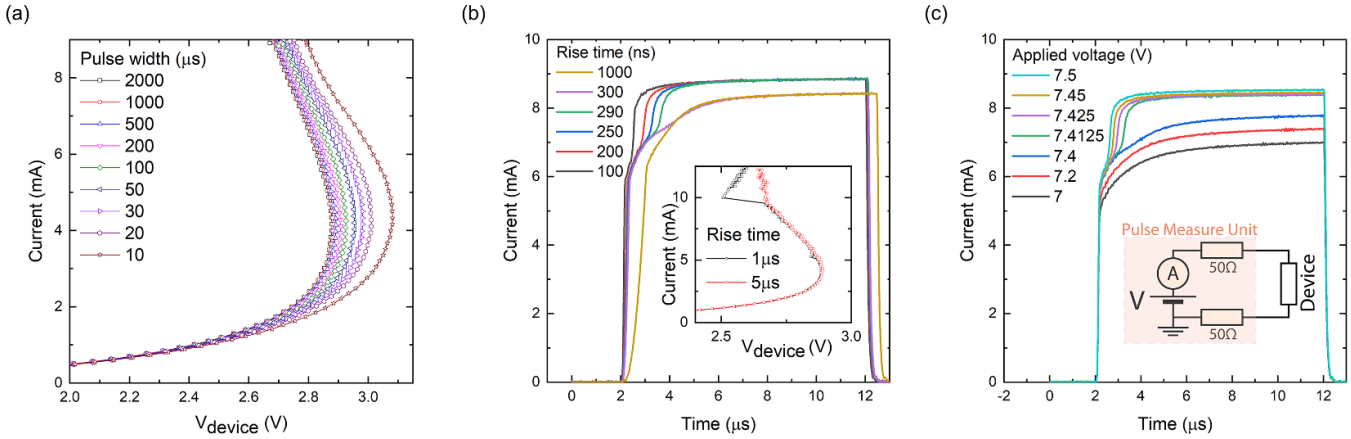

Figure 2. (a) Pulsed I–V measurement for different pulse widths (Δt). V_{device} was calculated using the I, applied V and a series resistance $R_s = 500\ \Omega$. Inset shows the V_{th} values for different Δt. (b), (c) Time-resolved I measurement during pulses with $V = 7.45$ V, $\Delta t = 10\ \mu$s, $R_s = 600\ \Omega$ and varying rise times (t_r). Below a certain t_r, a transition is observed to a resistance state than is even lower than that observed for the higher t_r's. Inset: Pulsed I–V measurement with different t_r's ($\Delta t = 1$ ms).

$t_r < 300$ ns if the voltage increase is large enough. By fixing the rise time while varying the applied voltage, we obtain a similar result (see figure 2(c)).

The observation of this additional transition could be explained by the formation of a high-current density domain, induced by the local increase of temperature, which has also been referred to as 'thermal filament' [13, 25, 58–64]. If the electrical relaxation time of the measurement circuit, which is determined by the resistance and capacitance of the circuit and the device, is longer than the thermal relaxation time, the temperature of the device can keep up with the electrical input and the device heats up gradually and relatively uniformly, reaching or closely approaching the steady-state during the increase of voltage. As the temperature of the material increases, its resistance goes down and a larger fraction of the applied voltage will drop on the series resistance (if there is one), limiting the electric field over the material. If, on the other hand, the electrical relaxation time is shorter than the thermal one, the temperature increase cannot keep up with the electric field increase and a higher electric field than in the previous case is reached across the device. In this scenario, field-activated transport, such as Poole-Frenkel conduction, which is sensitive to factors like roughness and inhomogeneities in the material, can be induced. Locally, large currents flow and high temperatures develop [58, 60, 63, 64].

3.2. Electrical oscillations

As mentioned in the introduction, CC-NDR can be used to make oscillators. To do this in our system, we place a load resistor (R_L) in series and a capacitor (C_p) in parallel to the device, as shown in the inset of figure 3(c). This circuit is much like that of the Pearson-Anson oscillator [65], a type of Van der Pol oscillator [66]. Under and applied voltage (V), V_{device} will increase gradually, until V_{th} is reached. The device then switches, its resistance dropping faster than the voltage can keep up (caused by the larger electrical RC), and the charge that was stored on the capacitor is discharged through the device. As a result of the discharge, the voltage over the device drops below V_h, after which the current decreases abruptly, allowing the temperature of the device to decrease and returning the device to its HR state. Subsequently, the capacitor is allowed to charge again, which marks the beginning of the next oscillation.

Figure 3(a) shows a series of measurements for various pulse voltages, in which we observe the self-oscillations. A pulse with a voltage that induces $V_{device} < V_{th}$ does not lead to oscillations (7 V in this example). For $V \geqslant 15$ V, the frequency and total power become too large for the device to be able to cool down in between two heating events. In this condition, the oscillations are damped and the system ends up in the high-temperature LR state. Note that the voltages are rather high, which is the result of the large series resistance we use (500 Ω) in order to observe the oscillations. Beside the applied voltage, two other parameters that play a role in the occurrence and frequency of oscillations in such a circuit are the load resistance and parallel capacitance [67, 68], as shown in figures 3(b) and (c).

One of the main issues for the design of self-oscillators is that the high temperatures, which can reach several hundreds of Kelvin locally [58, 60, 63, 64]), and large temperature gradients in the device can compromise the robustness of the oscillations and induce aging of the material. We expect that single phase epitaxial perovskite devices, which are not expected to show local phase changes at high temperatures, like these presented here, will show enhanced reliability. Therefore, we have investigated the endurance of these devices. An example of the sustained oscillations that are typically observed is shown in figure 4(a). We use the setup mentioned in the previous paragraph, but this time we change the parallel capacitor in order to vary the oscillation frequency. The results for four different devices with four different oscillation frequencies are shown in figure 4(b). We find that the oscillator endures at least 10^{11} cycles at 135 kHz, while the devices set to oscillate at lower frequencies are stable for at least 10^7 cycles. These values act as a lower limit for the actual endurance, as

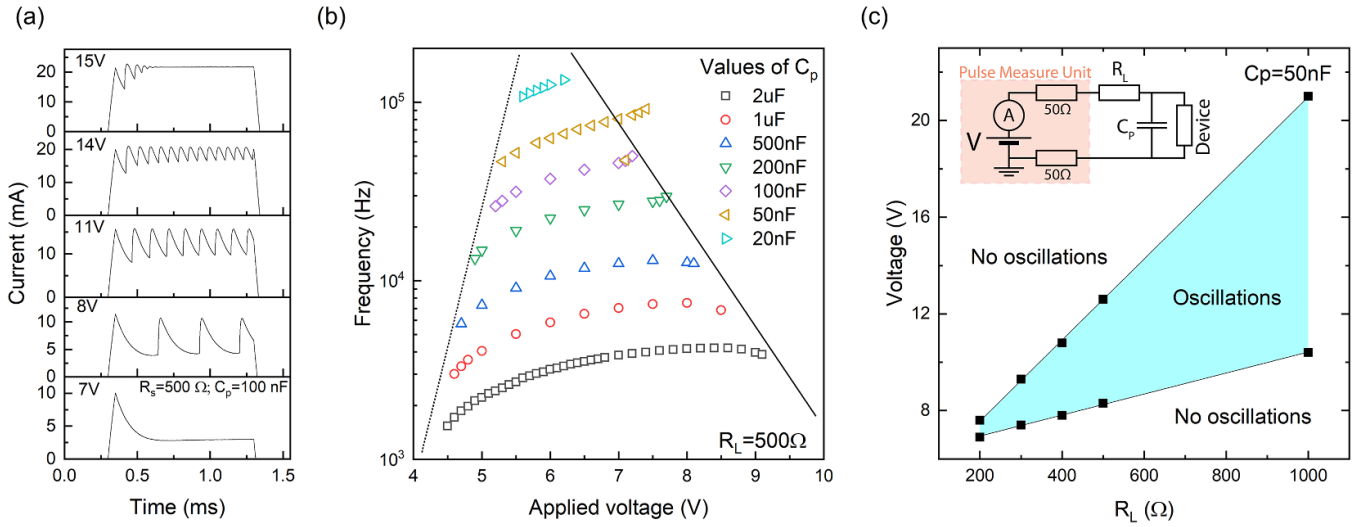

Figure 3. (a) Time-resolved current measurements showing oscillations when 7 V $<$ V $<$ 15 V, with V being the applied voltage (different from V_{device})), and with a constant R_L and C_p. (b) Oscillation frequency measured at varying applied voltage, for various values of C_p and a fixed R_L. Left and right of the coloured region, no oscillations were observed. (c) Example of range of values of applied voltage and R_L for which a circuit oscillates. Inset: Schematic circuit used to measure and manipulate the oscillations. The load resistance R_L and the parallel capacitance C_p are varied using a decade box, while another source of series resistance comes from the pulsed measure unit.

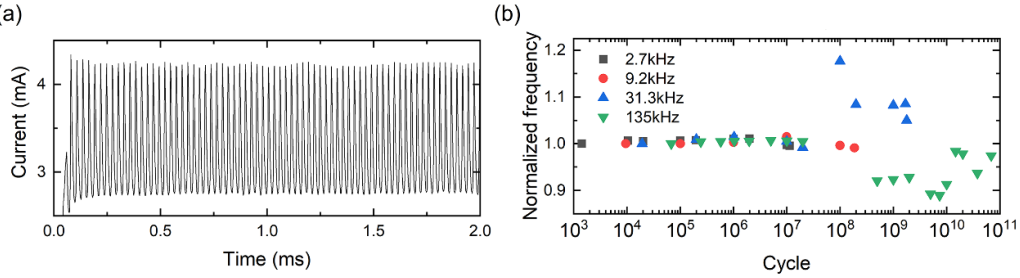

Figure 4. (a) Example of repeated self-oscillations. (b) Endurance test of four devices, each coupled with a different capacitance. The frequency was normalized to the values in the legend. For over 10^7 oscillations the frequency remains constant. The devices where turned off due to time constraints before they showed signs of breaking down.

the measurements were deliberately stopped after a few hours (or days, in the case of 135 kHz). The observed variability above 10^8 cycles could be due to a change in the temperature of the device or probe drift over the course of hours. We have not seen any device breaking down during or after cycling. As we varied the frequency by varying the parallel capacitance, the lower frequency oscillations are accompanied by larger discharge currents when the device switches. The fact that these devices can withstand these currents and the accompanying temperatures attests to the robustness of the devices.

4. Discussion

Several remarks can be made about these results. Firstly, for these devices to be used as selectors in memristor arrays, ideally $V_{th} < 1$ V, the ON-OFF ratio should be larger than 1000 and the current in the OFF-state as low as possible [69, 70]; these requirements likely being similar for efficient oscillators. These characteristics are less favourable in the devices described in this work than in devices made of NbO_2, VO_2 and TaO_x thus far, as expected, as these other systems have been optimized for this purpose for many years. The expectation is that optimization in $TbMnO_3$ can be accelerated as some of the insights from the work on binary oxides, such as the role of device geometry and dimensions, can directly be transferred to this material [59, 67, 71, 72].

Indeed, even though in NbO_2 and TaO_x the CC-NDR is often attributed to the Poole-Frenkel effect, the activation energies that are reported for the trap states in these cases are comparable to the activation energies that we have obtain in $TbMnO_3$. In particular, in the low-field regime, NbO_2 and TaO_x have shown activation energies in the ranges of 0.3–0.67 eV [9, 59, 73] and 0.24–0.44 eV [61], respectively, both depending on oxygen content. This compares well with the value of 0.26 eV shown in this work. Therefore, even if the origin of the NDR effect is different, the lesson learned on thermal management on the binary oxides can most likely be applied to this material.

Moreover, the large variety of polymorphs in transition metal simple oxides such as NbO_2 and TaO_x is a concern, as their electric properties (especially the

activation energy) depend strongly on their stoichiometry [9, 61, 73, 74] In contrast, in preparation for this work we have deposited $TbMnO_3$ under various growth conditions, yet the resulting activation energy is nearly identical (≈0.26 eV), as shown for the different curves in figure 1(c) and the supplementary material (available online at stacks.iop.org/JPhysD/55/335305/mmedia).

Several reports on NbO_2 [33, 75, 76] and TaO_x [39] indicate that a forming step is required to initiate threshold switching and fast oscillations in large devices. Forming confines the current in smaller volume filaments that can heat-up and cool-down faster, producing larger oscillation frequencies [70, 71, 77]. In this work we did not require a forming step; however, we did observe that, whenever we deliberately damaged a device by passing a high current (>100 mA) through it, the oscillation frequency would increase substantially. The damage is observed as a permanent change in the electrical behaviour of the device, as well as a visually damaged electrode. The increase in frequency could be explained either by the formation of a filament with different chemical composition or by the delamination of the electrode caused by the heat that is produced during the thermal runaway [58, 78, 79]. Both would lead to a smaller volume to be heated and, therefore, to a higher oscillation frequency. Compared to requiring forming steps or inducing damage, miniaturization of these device offers a more controlled way to obtain higher frequencies.

Additionally, as mentioned earlier, the voltages reported in this work include a voltage drop on the p–n junction at the interface between the $TbMnO_3$ film and the Nb-doped $SrTiO_3$ substrate. In order to operate the device at a lower voltage, this extra voltage drop is unwanted. Making use of a lateral device geometry, e.g. on non-doped $SrTiO_3$, or by making use of a bottom electrode that forms an ohmic interface with $TbMnO_3$, would both prevent this issue.

The load resistance and parallel capacitance that had to be added to make an oscillator do not have to be external. In this work they were, but an optimally-designed device could have the capacitance and load resistance included in the material properties and device geometry such that a single device can operate as oscillator.

Although no systematic study of the device reproducibility is performed in this work, many devices on the same film have shown the same or similar response, from the IV characteristics in figures 1(a)–(c) to the prolonged oscillations in figures 4(a) and (b). Over the course of two years, the same and different devices have been examined and have always provided the same or similar results. Further optimization of the devices is beyond the scope of this work.

Finally, coupling oscillators is of great interest to neuromorphic computing strategies [22, 31, 80, 81]. The coupling can be done electrically [31, 32, 81], but recently it was shown that these oscillators based on Joule heating can be coupled through temperature as well [82]. The phenomena shown here are also expected in other perovskites with similar electronic band structures, enhancing the prospects for combinations of different neuromorphic functionalities in a single compact heterostructure. Indeed, in studies about unrelated phenomena, several perovskite manganites have shown CC-NDR, albeit in bulk form or (well) below room temperature (e.g. the well-known manganite $Pr_{1-x}Ca_xMnO_3$) possibly all caused by Joule heating [15, 83, 84]. Also, several perovskites exist that show an insulator-metal transition, such as nickelates [85–87] and several manganites [88, 89], which would, just like in NbO_2 and VO_2, enhance the ON-OFF ratio of these devices. In addition, the transition temperature in those materials is tunable by composition [28, 85–87, 90] and strain [28, 87, 90], granting additional design flexibility.

5. Conclusion

In summary, we have shown that CC-NDR is found in thin films of $TbMnO_3$. All the experiments, including pulsed I–V measurements, are consistent with Joule heating as the origin of the NDR effect. A well-defined activation energy for electrical conduction, which does not change with the growth conditions or orientation of the material, has been measured, excluding the effect of defects or electron traps. Instead, the value of the activation energy fully agrees with the intrinsic band gap of $TbMnO_3$. As expected from the non-linear dependence of the conductivity with temperature in intrinsic semiconductors, the device produces current oscillations when embedded in a Pearson-Anson circuit. We found that the rate at which the voltage is applied has an influence on the final resistance of the device, which is consistent with the formation of high-temperature current constriction. The frequency of the electrical oscillations reaches up to 200 kHz in this work and the devices show a high endurance. The limits of the endurance have not yet been tested. This work could be a first step on the development of oxide perovskite heterostructures with combined neuromorphic functionalities.

Data availability statement

The data that support the findings of this study are openly available at the following URL/DOI: https://doi.org/10.34894/PY66WR.

Acknowledgments

We thank Cynthia Quinteros and Pavan Nukala for their discussions and contributions during this project and Arjun Joshua, Jacob Baas and Henk Bonder for technical support. Financial support by the Groningen Cognitive Systems and Materials Center (CogniGron) and the Ubbo Emmius Foundation of the University of Groningen is gratefully acknowledged.

Competing interest

The authors declare no competing interests.

ORCID iDs

M Salverda https://orcid.org/0000-0003-2275-4041

R P Hamming-Green https://orcid.org/0000-0001-6383-9733
B Noheda https://orcid.org/0000-0001-8456-2286

References

[1] Amerasekera A, Chang M-C, Seitchik J, Chatterjee A, Mayaram K and Chern J-H 1993 *IEEE Trans. Electron Devices* **40** 1836–44
[2] Berglund C and Klein N 1971 *Proc. IEEE* **59** 1099
[3] Altcheh L and Klein N 1973 *IEEE Trans. Electron Devices* **20** 801
[4] Zhou B Y and Ramanathan S 2015 *Proc. IEEE* **103** 1289–310
[5] Pickett M D and Stanley Williams R 2012 *Nanotechnology* **23** 215202
[6] Valmianski I, Wang P Y, Wang S, Ramirez J G, Guénon S and Schuller I K 2018 *Phys. Rev.* B **98** 195144
[7] Imada M, Fujimori A and Tokura Y 1998 *Rev. Mod. Phys.* **70** 1039
[8] Gibson G A 2018 *Adv. Funct. Mater.* **28** 1704175
[9] Funck C, Menzel S, Aslam N, Zhang H, Hardtdegen A, Waser R and Hoffmann-Eifert S 2016 *Adv. Electron. Mater.* **2** 1600169
[10] Gibson G A *et al* 2016 *Appl. Phys. Lett.* **108** 023505
[11] Kaplan T, Bullock D C, Adler D and Epstein D J 1972 *Appl. Phys. Lett.* **20** 439
[12] Knight S, Buehler E and Camlibel I 1972 *J. Appl. Phys.* **43** 3422
[13] Haubenreisser W, Löser W, Mattheck C, Möckel K and Steinbeiss E 1974 *Phys. Status Solidi* a **22** 427
[14] Fischer A, Pahner P, Lüssem B, Leo K, Scholz R, Koprucki T, Gärtner K and Glitzky A 2013 *Phys. Rev. Lett.* **110** 126601
[15] Biškup N, de Andrés A, Ochando I M and Casais M T 2006 *Phys. Rev.* B **73** 184404
[16] Arya S and Singh H 1979 *Thin Solid Films* **62** 353
[17] Cope R G and Goldsmid H J 1965 *Br. J. Appl. Phys.* **16** 1501
[18] Roy Bardhan A, Srivastava P and Bhattacharya D 1974 *Thin Solid Films* **24** S41
[19] Ielmini D and Ambrogio S 2020 *Nanotechnology* **31** 092001
[20] Burr G W *et al* 2017 *Adv. Phys.* X **2** 89
[21] Sebastian A, Le Gallo M, Khaddam-Aljameh R and Eleftheriou E 2020 *Nat. Nanotechnol.* **15** 529–44
[22] Chua L, Sbitnev V and Kim H 2012 *Int. J. Bifurcation Chaos* **22** 1250098
[23] Chicca E and Indiveri G 2020 *Appl. Phys. Lett.* **116** 120501
[24] del Valle J, Ramírez J G, Rozenberg M J and Schuller I K 2018 *J. Appl. Phys.* **124** 211101
[25] Goodwill J M, Ramer G, Li D, Hoskins B D, Pavlidis G, McClelland J J, Centrone A, Bain J A and Skowronski M 2019 *Nat. Commun.* **10** 1628
[26] Kumar S, Strachan J P and Williams R S 2017 *Nature* **548** 318
[27] Gao L, Chen P-Y and Yu S 2017 *Appl. Phys. Lett.* **111** 103503
[28] Andrews J L, Santos D A, Meyyappan M, Williams R S and Banerjee S 2019 *Trends Chem.* **1** 711
[29] Rozenberg M J, Schneegans O and Stoliar P 2019 *Sci. Rep.* **9** 11123
[30] Burr G W, Shenoy R S, Virwani K, Narayanan P, Padilla A, Kurdi B and Hwang H 2014 *J. Vac. Sci. Technol.* B **32** 040802
[31] Yi W, Tsang K K, Lam S K, Bai X, Crowell J A and Flores E A 2018 *Nat. Commun.* **9** 4661
[32] Pickett M D, Medeiros-Ribeiro G and Williams R S 2013 *Nat. Mater.* **12** 114
[33] Ascoli A, Slesazeck S, Mahne H, Tetzlaff R and Mikolajick T 2015 *IEEE Trans. Circuits Syst.* I **62** 1165
[34] Herzig M, Weiher M, Ascoli A, Tetzlaff R, Mikolajick T and Slesazeck S 2019 *J. Phys. D: Appl. Phys.* **52** 325104
[35] Müller K-H, Wolf M and Kammler F 1976 *Phys. Status Solidi* a **37** K201
[36] Brodkorb W and Haubenreisser W 1972 *Phys. Status Solidi* a **11** 755
[37] Brodkorb W and Haubenreisser W 1972 *Phys. Status Solidi* a **12** 655
[38] Goodwill J M, Gala D K, Bain J A and Skowronski M 2018 *J. Appl. Phys.* **123** 115105
[39] Gala D K, Sharma A A, Li D, Li D, Goodwill J M, Bain and J A and Skowronski M 2016 *APL Mater.* **4** 016101
[40] Mian M S, Okimura K and Sakai J 2015 *J. Appl. Phys.* **117** 215305
[41] Li S, Liu X, Nandi S K, Venkatachalam D K and Elliman R G 2015 *Appl. Phys. Lett.* **106** 212902
[42] Coll M *et al* 2019 *Appl. Surf. Sci.* **482** 1
[43] Chanthbouala A *et al* 2012 *Nat. Mater.* **11** 860
[44] Goossens A S, Das A and Banerjee T 2018 *J. Appl. Phys.* **124** 152102
[45] Bagdzevicius S, Maas K, Boudard M and Burriel M 2017 *J. Electroceramics* **39** 157
[46] Acevedo W R, Rubi D, Lecourt J, Lüders U, Gomez-Marlasca F, Granell P, Golmar F and Levy P 2016 *Phys. Lett.* A **380** 2870
[47] Guo R, Lin W, Yan X, Venkatesan T and Chen J 2020 *Appl. Phys. Rev.* **7** 011304
[48] Asamitsu A, Tomioka Y, Kuwahara H and Tokura Y 1997 *Nature* **388** 50
[49] Lu W, Sun Y, Zhao B, Zhu X and Song W 2006 *Solid State Commun.* **137** 288
[50] Jain H, Raychaudhuri A K, Ghosh N and Bhat H L 2007 *Phys. Rev.* B **76** 104408
[51] Daumont C J M, Mannix D, Venkatesan S, Catalan G, Rubi D, Kooi B J, De Hosson J T M and Noheda B 2009 *J. Phys.: Condens. Matter.* **21** 182001
[52] Venkatesan S, Daumont C, Kooi B J, Noheda B and De Hosson J T M 2009 *Phys. Rev.* B **80** 214111
[53] Farokhipoor S *et al* 2014 *Nature* **515** 379
[54] Park C, Seo Y, Jung J and Kim D-W 2008 *J. Appl. Phys.* **103** 054106
[55] Jin K, Zhai Y, Li H, Tian Y, Luo B and Wu T 2014 *Solid State Commun.* **199** 39
[56] Cui Y, Peng H, Wu S, Wang R and Wu T 2013 Complementary charge trapping and ionic migration in resistive switching of rare-earth manganite $TbMnO_3$ *ACS Appl. Mater. Interfaces* **5** 1213
[57] Cui Y, Wang C and Cao B 2005 *Solid State Commun.* **133** 641
[58] Goodwill J M and Skowronski M 2019 *J. Appl. Phys.* **126** 035108
[59] Wang Z, Kumar S, Philip. Wong H-S and Nishi Y 2018 *Appl. Phys. Lett.* **112** 073102
[60] Kumar S and Williams R S 2018 *Nat. Commun.* **9** 2030
[61] Goodwill J M, Sharma A A, Li D, Bain J A and Skowronski M 2017 *ACS Appl. Mater. Interfaces* **9** 11704
[62] Li D, Sharma A A, Shukla N, Paik H, Goodwill J M, Datta S, Schlom D G, Bain J A and Skowronski M 2017 *Nanotechnology* **28** 405201
[63] Nath S K, Nandi S K, Li S and Elliman R G 2019 *Appl. Phys. Lett.* **114** 062901
[64] Nandi S K, Nath S K, ElHelou A E, Li S, Liu X, Raad P E and Elliman R G 2019 *Adv. Funct. Mater.* **29** 1906731
[65] Pearson S and Anson H 1921 *Proc. Phys. Soc. London* **34** 204
[66] vander Pol B 1926 *London, Edinburgh Dublin Phil. Mag. J. Sci.* **2** 978
[67] Liu X, Li S, Nandi S K, Venkatachalam D K and Elliman R G 2016 *J. Appl. Phys.* **120** 124102
[68] Lalevic B and Shoga M 1981 *Thin Solid Films* **75** 199
[69] Li D, Goodwill J M, Bain J A and Skowronski M 2017 *Nanoscale* **9** 14139

[70] Wang Z, Kumar S, Williams R S, Nishi Y and Wong H-S P 2019 *Appl. Phys. Lett.* **114** 183501
[71] Liu X, Nandi S K, Venkatachalam D K, Belay K, Song S and Elliman R G 2014 *IEEE Electron Device Lett.* **35** 1055
[72] Cha E, Park J, Woo J, Lee D, Prakash A and Hwang H 2016 *Appl. Phys. Lett.* **108** 2014
[73] Wang Z, Kumar S, Wong H S and Nishi Y 2018 *Appl. Phys. Lett.* **112** 073102
[74] Jeong J, Aetukuri N, Graf T, Schladt T D, Samant M G and Parkin S S P 2013 *Science* **339** 1402
[75] Nandi S K, Li S, Liu X and Elliman R G 2017 *Appl. Phys. Lett.* **111** 202901
[76] Liu X, Li S, Nandi S K, Venkatachalam D K and Elliman R G 2016 *J. Appl. Phys.* **120** 124102
[77] Funck C, Hoffmann-Eifert S, Lukas S, Waser R and Menzel S 2017 *J. Comput. Electron.* **16** 1175
[78] Dittmann R, Muenstermann R, Krug I, Park D, Menke T, Mayer J, Besmehn A, Kronast F, Schneider C M and Waser R 2012 *Proc. IEEE* **100** 1979
[79] Münstermann R, Yang J J, Strachan J P, Medeiros-Ribeiro G, Dittmann R and Waser R 2010 *Phys. Status Solidi* **4** 16
[80] Chua L O 2005 *Int. J. Bifurcation Chaos* **15** 3435
[81] Romera M *et al* 2018 *Nature* **563** 230
[82] Velichko A, Belyaev M, Putrolaynen V, Perminov V and Pergament A 2018 *Solid-State Electron.* **141** 40
[83] Mercone S, Frésard R, Caignaert V, Martin C, Saurel D, Simon C, André G, Monod P and Fauth F 2005 *J. Appl. Phys.* **98** 023911
[84] Fisher B, Genossar J, Chashka K B, Patlagan L and Reisner G M 2006 *Appl. Phys. Lett.* **88** 152103
[85] Catalan G 2008 *Phase Transit.* **81** 729
[86] Torrance J, Lacorre P, Nazzal A, Ansaldo E and Niedermayer C 1992 *Phys. Rev.* B **45** 8209
[87] Catalano S, Gibert M, Fowlie J, Íñiguez J, Triscone J-M and Kreisel J 2018 *Rep. Prog. Phys.* **81** 046501
[88] Coey J M D, Viret M and von Molnár S 1999 *Adv. Phys.* **48** 167
[89] Salamon M B, Jaime M and Jaime M 2001 *Rev. Mod. Phys.* **73** 583
[90] Ogimoto Y, Nakamura M, Takubo N, Tamaru H, Izumi M and Miyano K 2005 *Phys. Rev.* B **71** 3